Ocean Engineering 36 (2009) 368–376

Contents lists available at ScienceDirect

Ocean Engineering

journal homepage: www.elsevier.com/locate/oceaneng

Modeling the near-field effects of the worst-case tsunami in the Makran subduction zone

Mohammad Heidarzadeh [a,*], Moharram D. Pirooz [a], Nasser H. Zaker [b]

[a] School of Civil Engineering, College of Engineering, University of Tehran, Enghelab Ave., P.O.Box: 11155-4563, Tehran, Iran
[b] Graduate Faculty of Environment, University of Tehran, Tehran, Iran

ARTICLE INFO

Article history:
Received 20 May 2008
Accepted 8 January 2009
Available online 20 January 2009

Keywords:
Tsunami hazard
Makran subduction zone (MSZ)
Worst-case scenario
Numerical modeling
Runup calculations

ABSTRACT

As a first step towards the development of inundation maps for the northwestern Indian Ocean, we simulated the near-field inundation of two large tsunami in the Makran subduction zone (MSZ). The tsunami scenarios were based on large historical earthquakes in the region. The first scenario included the rupture of about 500 km of the plate boundary in the eastern MSZ, featuring a moment magnitude of M_w 8.6. The second scenario involved the full rupture of the plate boundary resulting from a M_w 9 earthquake. For each scenario, the distribution of tsunami wave height along the coastlines of the region is presented. Also, detailed runup modeling was performed at four main coastal cities in the region for the second scenario. To investigate the possible effect of splay fault branching on tsunami wave height, a hypothetical splay fault was modeled which showed that it can locally increase the maximum wave height by a factor of 2. Our results showed that the two tsunami scenarios produce a runup height of 12–18 m and 24–30 m, respectively. For the second scenario, the modeled inundation distance was between 1 and 5 km.

1. Introduction

The great Sumatra-Andaman tsunami of 2004 has awakened the attention of the scientific community to tsunami hazards in the Indian Ocean Basin (Okal and Synolakis, 2008). This earthquake was produced by the upper part of the Sunda subduction zone which due to its age and convergence rate, was believed to be among the least likely zones to produce such a giant earthquake (Geist et al., 2006). Stein and Okal (2007) re-examined great earthquakes worldwide and showed that there is no strong correlation between the maximum size of subduction earthquakes and the convergence rate and age of the subduction zone. They proposed that the correlation of maximum magnitude to convergence rate or age was a specious result because of the limited historical and instrumental record. Similar statements were made by McCaffrey (2007).

Okal (2007) proposed that the maximum earthquake size expected from a subduction zone depends on the length of a continuous fault system along a convergent plate boundary. This result is of the utmost importance in view of tsunami hazard assessment, and emphasizes the need for reassessing the tsunami hazard associated with subduction-related tsunamigenic earthquakes worldwide.

According to several tsunami catalogs, tsunami in the Indian Ocean basin have been generated by two subduction zones in this region, namely the Sunda subduction zone located offshore Indonesia, responsible for the 2004 Indian Ocean tsunami, and the Makran subduction zone (MSZ) in the northwest Indian Ocean (Fig. 1). The MSZ is formed by the northward subduction of the Arabian plate beneath the Eurasian one (Fig. 1). This zone extends east from the Strait of Hormoz in Iran to near Karachi in Pakistan with a length of about 900 km. MSZ was the site of a major earthquake on November 27th, 1945 (M_w 8.1), which was accompanied by a significant regional tsunami, with runup in the 4–5 m range (Ambraseys and Melville, 1982) and about 4000 fatalities (Heck, 1947). Recently, Heidarzadeh et al. (2008a, b, 2009) studied historical tsunami in this region and presented preliminary estimations of the tsunami hazard associated with the MSZ. By reviewing and analyzing large historical earthquakes along the Makran coast, Okal and Synolakis (2008) defined two worst-case scenarios for the possible mega-thrust earthquakes in the MSZ and investigated their far-field effects across the Indian Ocean basin.

Since the development of credible worst-case tsunami hazard scenarios is necessary for the planning of mitigation strategies; in this paper, we focused on the modeling of the near-field effects of the worst-case scenarios in the Makran region. Here, we use the term *worst-case scenario* as the maximum plausible earthquake and tsunami in the study area. Worst-case scenarios have been the basis for tsunami hazard assessments for many vulnerable

* Corresponding author. Tel.: +98 9111134123; fax; +98 21 22222407.
E-mail address: heidarz@ut.ac.ir (M. Heidarzadeh).

0029-8018/$ - see front matter © 2009 Elsevier Ltd. All rights reserved.
doi:10.1016/j.oceaneng.2009.01.004

coastlines across the world. Tsunami mitigation measures are often based on the maximum water elevations and the maximum inundation distances obtained from the worst-case scenarios. For example, Synolakis (2003) reported that inundation maps for the west coast of the United States are being developed taking into account worst-case scenarios. Different methods have been employed to calculate worst-case scenarios for various tectonic settings. To define such scenarios for subduction zones, the current state-of-the-art method uses a combination of the concepts described by Plafker (1972), Ando (1975), and Okal (2007). This method, previously used by Okal and Synolakis (2008), will be discussed in more detail later in the paper.

The worst-case earthquakes used in this study are the same as those defined by Okal and Synolakis (2008) in their far-field study. We modeled the propagation and inundation of each worst-case scenario, and present here the distribution of maximum tsunami runup and horizontal inundation along various coasts in the region. In order to validate our numerical modeling of tsunami, the well-known Makran earthquake and tsunami of 1945 was modeled first. The results of our study will assist in developing tsunami preparedness strategies in the northwestern Indian Ocean where the tsunami hazard is inadequately understood.

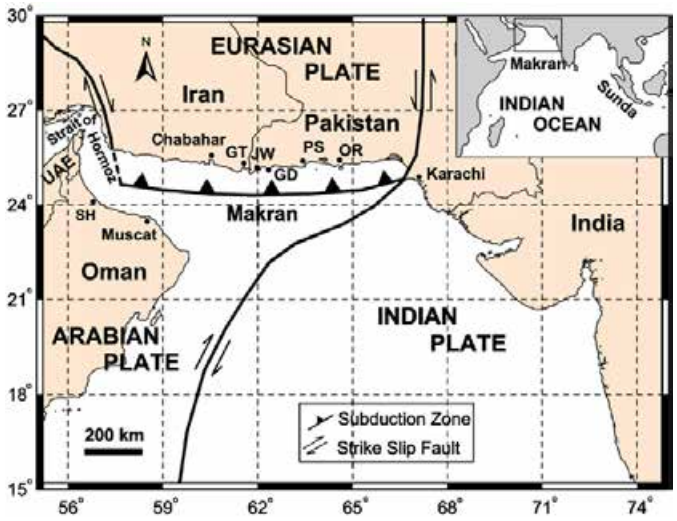

Fig. 1. Location map and tectonic setting of the makran subduction zone (MSZ). The inset shows the MSZ compared to the entire Indian Ocean region. Abbreviations: GT, Gwatar; JW, Jiwani GD, Gwadar; PS, Pasni; OR, Ormara; SH, Suhar.

2. Worst-case scenario earthquakes

We first review the history of large earthquakes in the MSZ and examine which sections of the plate boundary can produce large earthquakes. Historical earthquakes in the MSZ were studied by some authors including Quittmeyer and Jacob (1979), Page et al. (1979), Ambraseys and Melville (1982), Byrne et al. (1992), and most recently by Okal and Synolakis (2008). A review of these studies indicates that the Makran region experienced at least seven large earthquakes ($M>7$) in the past 500 years rupturing the plate boundary in four different segments as shown in Fig. 2 which is modified from Okal and Synolakis (2008, Fig. 7), and Byrne et al. (1992, Fig. 6). Also, the information of these large earthquakes is summarized in Table 1.

As indicated in Fig. 2 by a question mark, the 1483 earthquake in the western Makran is uncertain, and some authors believe that the western Makran is entirely aseismic. However, Byrne et al. (1992) believed that the absence of plate boundary events in western Makran may indicate that the plate boundary is currently locked and experiences great earthquakes with long repeat times. Hence, we take into account possible rupture in western Makran for the present worst-case study.

Following the 2004 Indian Ocean tsunami and taking into account the lessons learned from this maga–tsunami, Okal (2007) proposed that the maximum earthquake size expected from a subduction zone depends on the length of a continuous fault system along a convergent plate boundary. This continuous segment is about 500 km (blocks A, B, and C in Fig. 2) for the MSZ as the segmentation of this subduction zone was confirmed by Byrne et al. (1992). Therefore, the simultaneous rupture of blocks A, B, and C is considered as the first worst-case scenario in this study.

By studying historical earthquakes produced by the Nankai subduction zone in southwest Japan, Ando (1975) demonstrated that the rupture pattern along a given segmented subduction zone is unpredictable, and can vary from a single segment rupture to a full rupture of all segments at the same time. Okal and Synolakis (2008) reported that the concept proposed by Ando (1975) has recently been upheld in other subduction zones across the

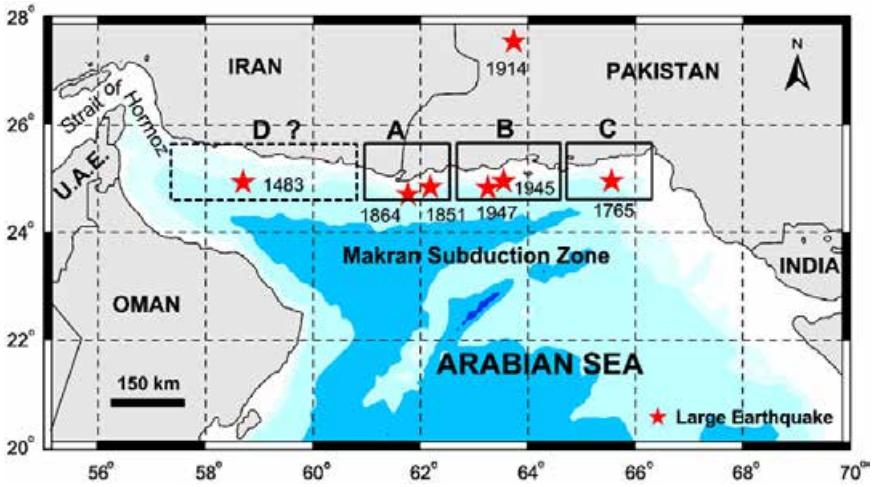

Fig. 2. Large historical earthquakes in the MSZ (filled stars). The four blocks A–D, are different segments of the plate boundary ruptured due to the large earthquakes. Modified from Okal and synolakis (2008, Fig. 7) and Byrne et al. (1992, Fig. 6).

world. Therefore, as the second worst-case scenario, we consider the simultaneous rupture of all of the plate boundary segments (blocks A, B, C, and D in Fig. 2).

The other method considered here for developing the worst-case scenarios, is the one proposed by Plafker (1972). Based on his work on the 1964 Alaskan and 1960 Chilean tsunami, Plafker (1972) showed that splay faulting can strongly increase the seafloor uplift and consequently intensify the near-field runup of tsunami during large subduction earthquakes. Therefore, we have also modeled the possible effect of splay faulting for our worst-case study.

To estimate the return periods and likelihood of the two earthquake scenarios, we refer to the study by Heidarzadeh et al. (2008b) who presented a probabilistic seismic hazard assessment for the Makran region based on its previous seismicity. Their study suggests a return period of about 250 years for a 1945-type earthquake (M_w 8.1) which agrees with the previous estimates made by Page et al. (1979) and Byrne et al. (1992). Based on the study by Heidarzadeh et al. (2008b), the return period of a M_w 8.3 earthquake is about 1000 years, and the probability of having such an earthquake in the next 100 years is about 10%. It is evident that the two earthquake scenarios studied here are very rare events having far longer return periods and far less likelihoods.

3. Source modeling and calibration

The tsunami modeling process can be divided into three parts: generation, propagation, and runup (Synolakis, 2003). Generation modeling forms the first stage in the modeling of tsunami, and includes the calculation of the initial disturbance of ocean surface due to the earthquake-triggered deformation of the seafloor using the seismic parameters.

The algorithm of Mansinha and Smylie (1971) was used to calculate the seafloor deformation. This algorithm is based on seismic parameters that include the strike, dip, and slip angles, the amount of slip, the dimensions of the ruptured area (length and width), and the earthquake depth. For each scenario, empirical equations were used to estimate the corresponding earthquake magnitude of each fault rupture followed by calculation of the rupture width and surface displacement (Wells and Coppersmith, 1994). We validated the predictions of the empirical equations using the available seismic parameters of the 1945 event. The only instrumentally recorded large earthquake at Makran is the event of 1945 (M_w 8.1) rupturing approximately one-fifth of the plate boundary and causing about 7 m of slip (Byrne et al., 1992). Table 2 presents the source parameters for the two earthquakes that we evaluate in this study. For the second scenario, a two-segment fault rupture was considered. A change in fault strike between the eastern and western parts of the MSZ has been confirmed by Byrne et al. (1992) who studied great thrust earthquakes in the MSZ. As shown in Table 2, the two earthquakes feature seismic moments of about 1.95×10^{22} Nm (1.95×10^{29} dyne $\times$ cm) and 1.01×10^{23} Nm (1.01×10^{30} dyne $\times$ cm), respectively. The seismic moment of the 2004 Sumatra earthquake was about 1.2×10^{30} dyne $\times$ cm (Stein and Okal, 2007).

Fig. 3 presents the results of tsunami source modeling for both scenarios. Scenario 1 and 2 produce maximum uplift of about 4.5 and 9 m on the seafloor, respectively. The results of dislocation modeling nearly agree with the average uplift caused by some similar actual earthquakes worldwide including the 2004 Indian Ocean tsunami (M_w 9.3, L = 1200–1300 km, average uplift ~12 m, after Stein and Okal, 2007; Sibuet et al., 2007), and 1964 Alaskan tsunami (M_w 9.2, L = 500–800 km, average uplift ~4.5 m, after Plafker, 1972). We emphasize that our results only agree with the average uplift observed during aforesaid tsunami. Plafker (1972) reported a maximum uplift of about 12 m locally produced by a splay fault during the 1964 Alaskan earthquake. In addition, more than 14 m of uplift also was reported in some areas due to the 2004 Indian Ocean tsunami caused by splay faulting (Plafker et al., 2007). In both cases, slip on a splay fault was responsible for these extraordinary uplifts, and thus it is necessary to consider possible splay faulting for worst-case tsunami modeling.

4. Propagation and runup modeling and validation

The numerical model TUNAMI-N2 was used for the simulation of propagation and coastal amplification of long waves. The model was developed by Nobuo Shuto and Fumihiko Imamura of the

Table 1
Summary of the information of the past large earthquakes in the MSZ.

No.	Date (yyyy–mm–dd)	Latitude (°N)	Longitude (°E)	M_s[a]	M_w[b]	Intensity (MM)[c]	Focal depth (km)
1	1483–??–??	24.90	57.90			10	
2	1765–??–??	25.40	65.80			8–9	
3	1851–04–19	25.10	62.30			8–9	
4	1864–??–??	25.12	62.33			6–8	
5	1914–??–??	29.70	63.80	7.0			
6	1945–11–27	24.50	63.00		8.1		25.0
7	1947–08–05	25.10	63.40		7.6		35.0

[a] Surface wave magnitude.
[b] Moment magnitude.
[c] Modified Mercalli.

Table 2
Source parameters of the two worst-case scenario earthquakes in the MSZ.

Scenario	Blocks	M_w	Segment	Length (km)	Width (km)	D[a] (m)	Depth (km)	Dip (deg.)	Slip (deg.)	Strike (deg.)	Moment (N m)[b]
1	A-B-C	8.6	1	500	100	13	25	7	90	265	1.95×10^{22}
2	A-B-C-D	9.0	1	500	150	25	25	7	90	265	1.01×10^{23}
			2	400	150	25	25	7	90	280	

[a] Displacement.
[b] The rigidity of the earth is considered to be 3×10^{10} N m^{-2}.

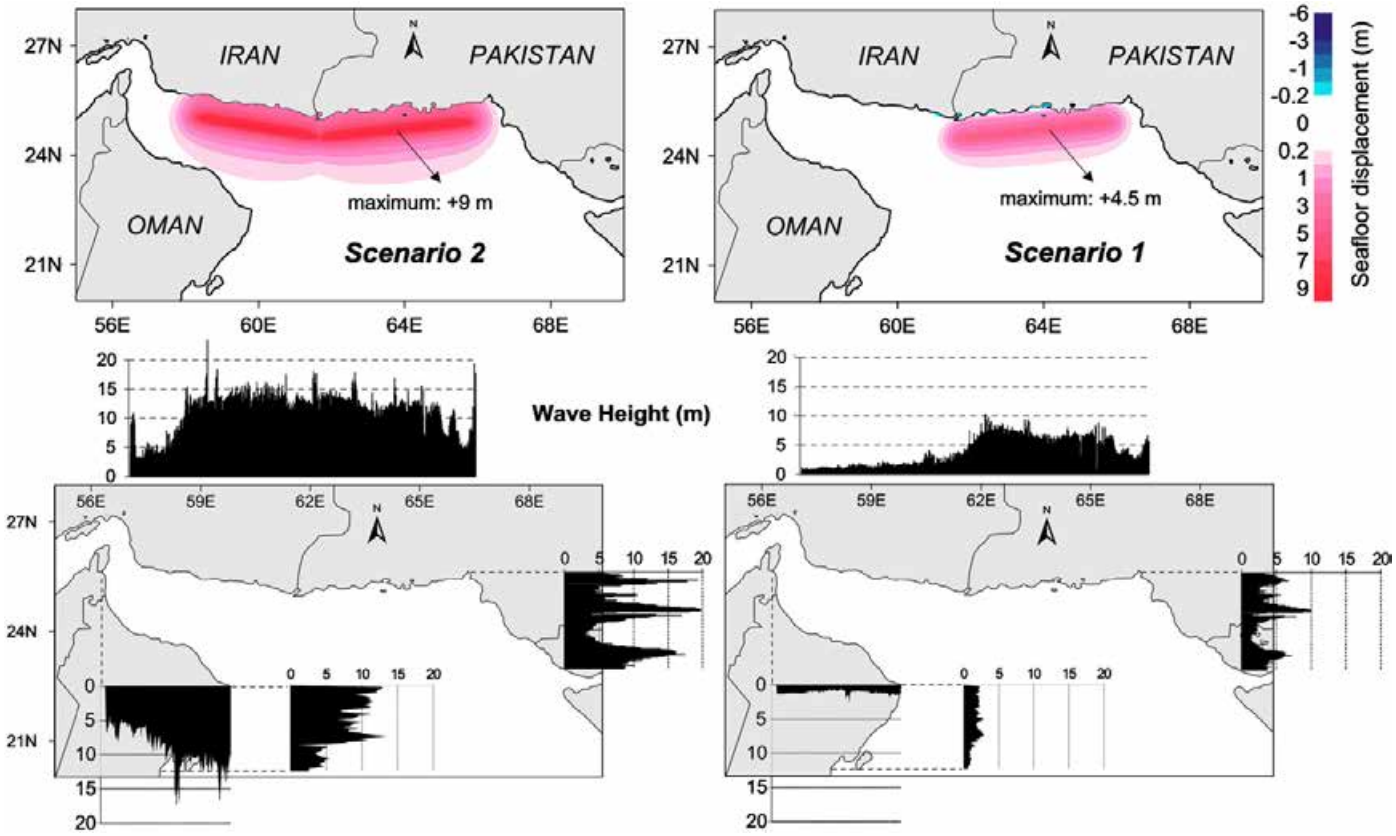

Fig. 3. Seafloor uplift due to the two worst-case earthquakes along with the distribution of maximum positive tsunami wave heights along various coasts.

Disaster Control Research Center in Tohoku University (Japan) through the Tsunami Inundation Modeling Exchange (TIME) program (Goto et al., 1997). TUNAMI-N2 is one of the key tools for numerical modeling of wave propagation and coastal amplification of tsunami in relation to different initial conditions (Yalciner et al., 2004). A similar methodology is used in the numerical model Method Of Splitting Tsunami (MOST) developed by Titov and Synolakis (1997). TUNAMI-N2 and MOST are nonlinear shallow water codes that have yielded satisfactory agreement with laboratory and field data (Yeh et al., 1996).

We used an 833×444 grid and 369852 grid points in our computational domain. The time step was 1.0 s to satisfy the stability condition. The duration of tsunami propagation was 3 h. Bathymetry data provided through the GEBCO digital atlas (General Bathymetric Chart of the Oceans) was applied in this study (IOC et al., 2003). As runup modeling is not applicable to large computational domains, we calculated the maximum positive tsunami heights along the coast which give a reasonable approximation of the runup heights (Tinti et al., 2006; Yalciner et al., 2004).

In order to verify numerical modeling of tsunami, we modeled the 1945 Makran tsunami, the only instrumentally recorded tsunamigenic earthquake in the MSZ and compared our results with historical observations. To model seafloor deformation due to this earthquake, the seismic parameters of the 1945 Makran earthquake (M_w 8.1), estimated in the study by Byrne et al. (1992), were used. Using these parameters, the maximum modeled seafloor deformation was about 2 m agreeing with the existing reports about the uplift of the 1945 event (e.g., Page et al., 1979).

Fig. 4 presents the modeled distribution of the 1945 tsunami wave heights along different coastlines. The wave height data of the 1945 tsunami are poor and no tide gauge record was available. However, we were able to collect some data about the tsunami wave heights along different parts of the Makran coast. According to Ambraseys and Melville (1982), tsunami wave height was about 4–5 m in Pasni, and about 1.5 m in Karachi. Also, they reported that the tsunami was observed along Makran coasts of Iran and Oman, but no damage and loss of life were reported from these coasts. Other authors reported wave heights of 12–15 m at Pasni due to the 1945 tsunami (e.g., Berninghausen, 1966). Heidarzadeh et al. (2008a) presented evidence that the Makran tsunami of 1945 was possibly associated with other phenomena like landslides or splay faults, and attributed the huge runup of 12–15 m to them. Based on their detailed runup modeling, Heidarzadeh et al. (2008a) concluded that a tectonic source for the 1945 tsunami is capable of producing 4–5 m of runup in the Pasni area. This is in agreement with the report by Ambraseys and Melville (1982).

According to our modeling results (Fig. 4), the distribution of tsunami wave height along various Makran coasts reproduces most features of the historical observations during the 1945 event. Our modeling successfully reproduced the observed wave height of 4 to 5 m at Pasni as well as 1.5 m in Karachi. In addition, Fig. 4 shows that the simulated wave heights at the southern coast of Iran and northern coast of Oman are less than 1 m. Thus, it is reasonable that there were few reports of wave inundation during the 1945 event in these areas.

To further examine the accuracy of the numerical modeling, we performed runup calculations for one coastal site, Pasni, using high-resolution bathymetry and topography data. We repeated the modeling scheme described above to calculate the runup heights in Pasni. The nested grid version of TUNAMI-N2, known as TUNAMI-N3, was employed. It solves the linear form of long wave equations in spherical coordinates in the largest domain, the deep sea, and nonlinear shallow water equations in Cartesian coordinates in smaller domains with finer grids.

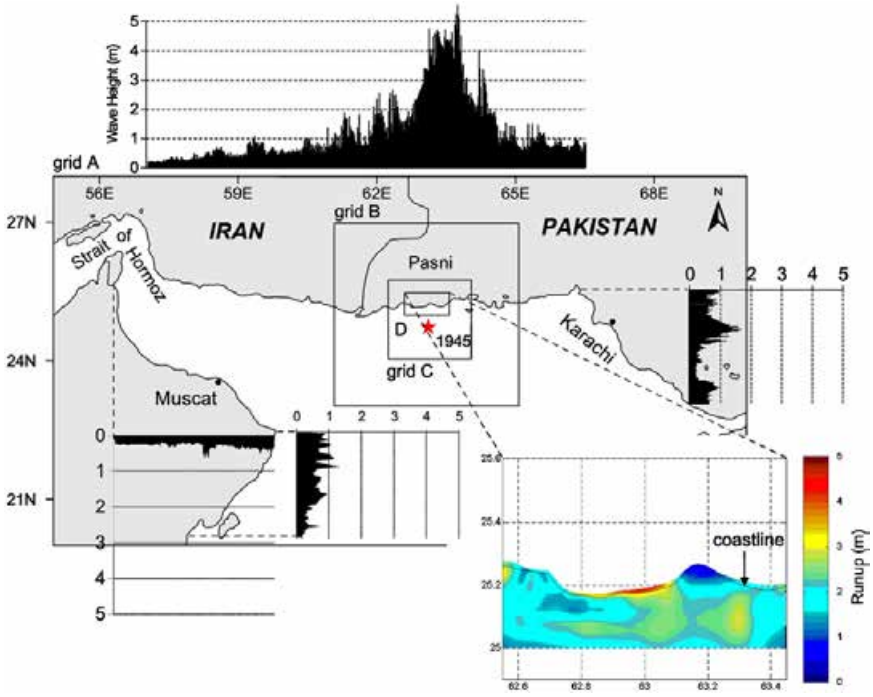

Fig. 4. Distribution of maximum tsunami wave heights in various makran coasts due to the makran tsunami of 1945 along with runup calculations in Pasni (after Heidarzadeh et al., 2008b, 2009).

A set of 4-level nested grids was used (grid set of ABCD in Fig. 4), where the grid resolution increases in the coastal areas. The first grid, A, covers the entire MSZ between 55–70°E and 20–28°N with a grid spacing of 2500 m. For the region D, where the inundation of tsunami over dry land is permitted, the resolution of the bathymetry and topography data was about 100 m. The result of the runup calculations in Pasni is shown in Fig. 4. The maximum simulated runup height was about 5 m which is in agreement with both historical observations and results of maximum tsunami heights along the coast.

5. Results

Similar to the previous section, TUNAMI-N2 was used to calculate the maximum positive tsunami heights along the coast for the whole computational domain, and TUNAMI-N3 for runup calculations along some selected coasts. Four sets of 4-level nested grids were used to calculate the tsunami runup in the four coastal cities namely Chabahar, Pasni, Muscat, and Karachi (Fig. 5). As shown, the grid sets of AB1C1D1, AB2C2D2, AB3C3D3, and AB4C4D4 were used to calculate the tsunami runup in the aforesaid coastal cities, respectively.

Fig. 3 presents the distribution of the maximum positive tsunami heights along the various Makran coasts for both scenarios. The results of detailed inundation modeling in the selected coastal sites are shown in Fig. 5 for the second scenario. Modeling results show that the tsunami will reach a height of about 6–9 m for the first scenario and 12–15 m for the second one.

For the first scenario, the resulting tsunami will have the greatest impact on the southern coast of Pakistan and relatively moderate effects on the remaining coasts. The tsunami wave height is up to 10 m along the southern coast of Pakistan and 1.5–3 m along the others. The tsunami generated by the first scenario earthquake appears to cause large amounts of inundation along the southern coast of Pakistan and some parts of the southern coast of Iran. This pattern can be attributed to the effect of directivity of tsunami waves (Ben–Menahem and Rosenman, 1972). Due to this effect, most of the tsunami's energy travels perpendicular to the strike of the fault in the far-field. However, a relatively strong directivity effect is also expected in the near-field. Therefore, for the first scenario, most of the tsunami's energy propagates in the north–south direction focusing on the southern coast of Pakistan in the north direction, and also propagating towards the open ocean in the south direction (Fig. 3). In Fig. 3,it can also be observed that in northern Oman where the average amplitude of tsunami is about 1.5 m, some areas adjacent to Muscat experience amplitude of up to 3 m.

Modeling results demonstrate that the second scenario earthquake is capable of producing a tsunami comparable to the 2004 Indian Ocean tsunami. The tsunami wave height is more than 10 m along nearly all of the costal areas in the region, and is about 15 m along nearly half of the coastlines (Fig. 3). The average wave height is between 12 and 15 m. Again, significant wave amplification is evident in some coastal sites including near Muscat and south of Karachi.

Based on the results of inundation modeling (Fig. 5), the maximum horizontal penetration of the tsunami is between 1.5 and 5 km in three coastal sites in the northern Makran (Chabahar, Pasni, and Karachi), and is about 1–3 km along the Omani coast. According to the local bathymetry and topography, shown in Fig. 5, it is clear that the greatest inundation occurs along low-lying coastlines. These huge inundation lengths are far greater than those of an ordinary tsunami, and are comparable only with those of a large tsunami like the 2004 event.

It is evident that such waves and the associated long inundation distances are capable of producing a real tragedy. Almost a half-million people live in the near field of a potential Makran tsunami which can be many more if the city of Karachi (11 million) is included in that region.

6. Modeling of possible splay fault branching

Plafker (1972) showed that the observed large local seafloor deformations during the 1960 Chilean (M_w 9.5) and

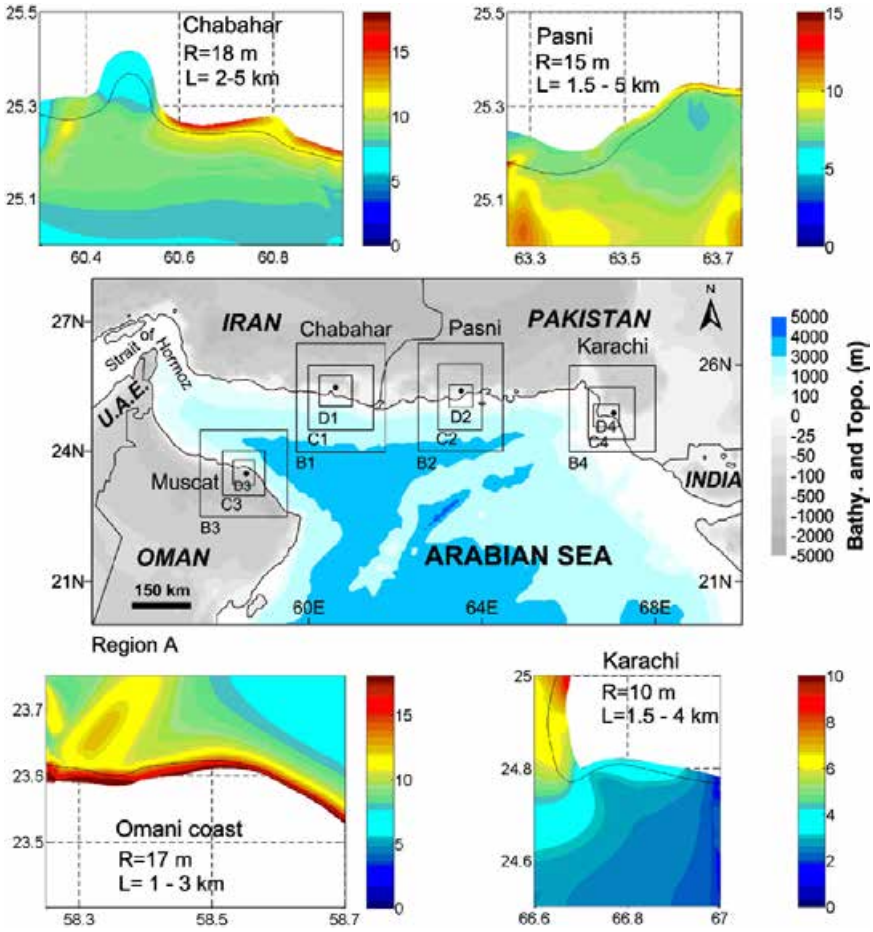

Fig. 5. The nested grid system used for inundation modeling in the selected areas along with the results of inundation modeling for the second scenario. Abbreviations: R, runup; L, inundation distance.

1964 Alaska (M_w 9.2) earthquakes were produced by the branching of splay faults from the main plate boundaries. According to Plafker (1972), splay faults are steeply-dipping faults that branch upward from the plate boundary at depth and steepen as they approach the surface (Fig. 6a). As an example, a displacement of about 8 m along a splay fault during the 1964 Alaskan earthquake was reported by Plafker (1972). Similar observations were also reported from other large subduction earthquakes, e.g., the 2004 Indian Ocean earthquake and tsunami (Plafker et al., 2007) and the 1946 Nankai earthquake and tsunami (Cummins and Kaneda, 2000). Based on the above observations, Plafker et al. (2007) and Sibuet et al. (2007) concluded that in the near-field, the tsunami source can be more complicated than a simple rupture on a mega-thrust, and that splay faults must be taken into account to understand the behavior of mega-thrust earthquakes. Due to splay faulting, the initial wave at the tsunami source can be higher and closer to the shore (Plafker et al., 2007) consequently producing larger runup in the near-field and shorter tsunami travel time to the coastline.

As the two scenarios considered in this study are for large mega-thrust earthquakes, branching of the plate boundary is likely. Furthermore, Heidarzadeh et al. (2008a) presented evidence that a splay fault may have been responsible for the huge observed runup of 12–15 m during the Makran tsunami of 1945. Also, Mokhtari et al. (2008) clearly showed splay faulting in the MSZ based on 2D seismic reflection data. Hence, it is necessary to investigate the effects of possible splay faulting on the tsunami scenarios. To do so, we repeat the modeling scheme described above for the first scenario earthquake with the assumption that a splay fault branches from the plate boundary during the earthquake. A hypothetical splay fault inspired by the 1946 Nankai and 1960 Chilean earthquakes was assumed to branch during the first scenario earthquake. Table 3 presents the seismic parameters of the splay fault and the main plate boundary slips for this new earthquake. We note that the seismic moment of this earthquake was kept unchanged and was the same as that of the first scenario (Table 3). Therefore, due to the slip on the splay fault, the maximum slip on the main plate boundary was reduced.

Using the database of Makran earthquakes (Heidarzadeh et al., 2008b), an approximation of the Makran plate boundary at depth is shown in Fig. 6a. The seafloor deformation due to the new earthquake is presented in Fig. 6b and c. As shown, the uplift was greatly increased locally along the splay fault. The maximum seafloor uplift due to the first earthquake scenario was about 4.5 m (solid line—Fig. 6b), which was raised to 7.2 m due to the presence of the splay fault. However, Fig. 6b and c shows that the increase in the amount of uplift is limited to the areas close to the splay fault.

Results of tsunami modeling (Fig. 6d) reveal that the possible splay faulting during large mega-thrust earthquakes in the MSZ can locally increase the maximum wave height by nearly a factor of 2. Based on Fig. 6d, the maximum simulated wave height is about 12 m in the vicinity of the splay fault, while it was about 6 m at the same location in the previous simulation. Similar to the

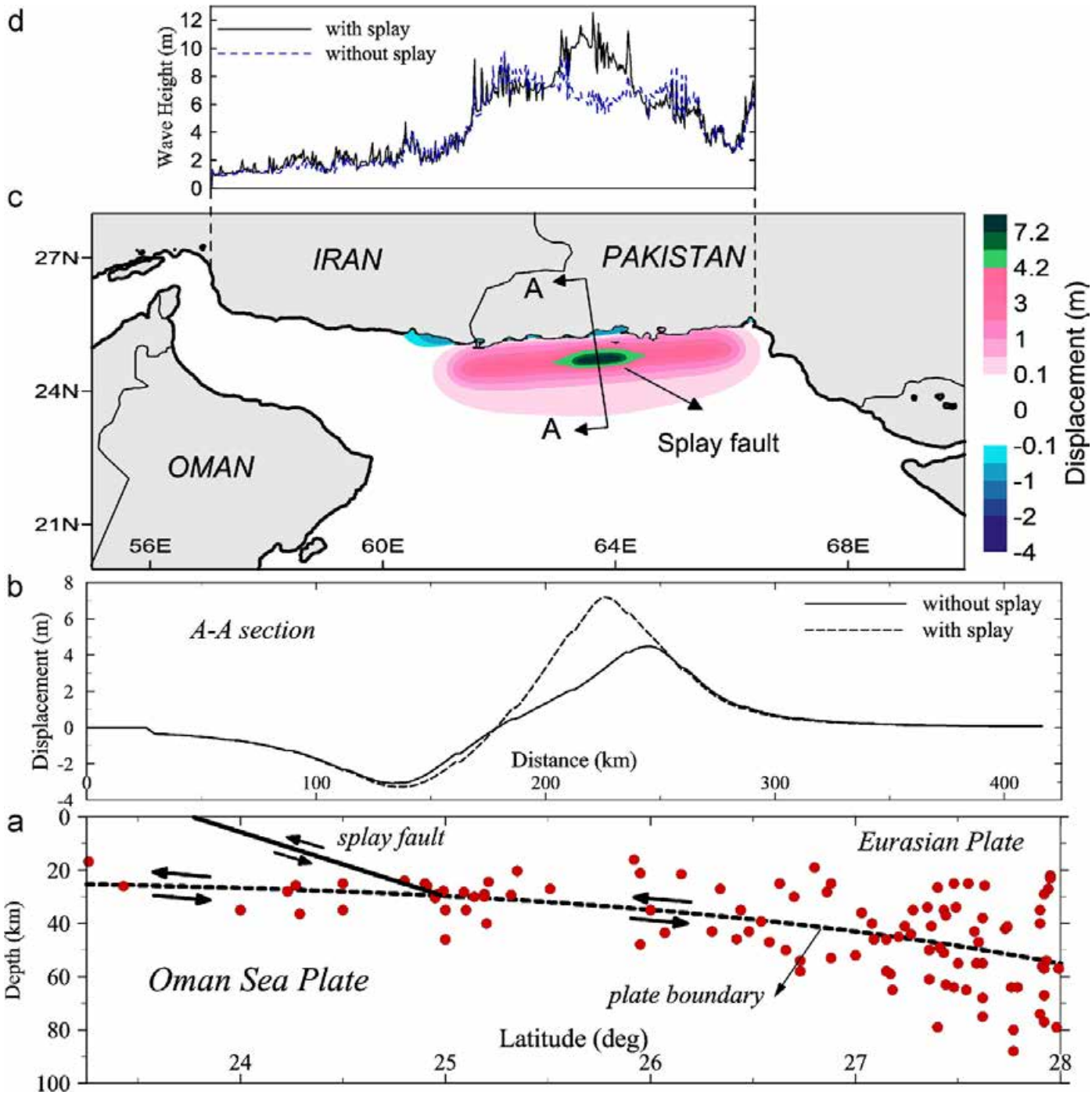

Fig. 6. The effect of a hypothetical splay fault on the tsunami wave height. Shown are: approximation of the plate boundary (a) cross section (b) and plan (c) of the seafloor deformation; and tsunami wave height (d).

Table 3
Source parameters used for modeling of the first scenario with considering a hypothetical splay fault.

Scenario	Blocks	Segment	Length (km)	Width (km)	D[a] (m)	Dip (deg.)	Slip (deg.)	Strike (deg.)	Moment (N m)[b]
1	A-B-C	Splay fault	100	50	10	30	90	265	1.95×10^{22}
		Main plate boundary	500	100	12	7	90	265	

[a] Displacement.
[b] The rigidity of the earth is assumed 3×10^{10} N m^{-2}.

seafloor uplift pattern, the effect of splay faulting on the distribution of tsunami wave height is localized to the vicinity of the splay fault.

The above results are consistent with the observations of tsunami runup during some actual large tsunami. For example, Plafker et al. (2007) reported that the peak runup was as high as

39 m west of Banda Aceh during the 2004 Indian Ocean tsunami, while they were about 5–12 m along the north coast and 7–20 m along the west coast of Indonesia. Plafker et al. (2007) concluded that alternate sources, such as secondary intraplate faults, may have contributed to the tsunami in addition to interplate slip on the Sumatra mega-thrust. In addition, Legg et al. (2004) reported that recent observations of tsunami runup following large earthquakes worldwide suggest that runup values predicted from simple elastic dislocation models of tectonic deformation underestimate the observed peak runup values by a factor of two or more.

7. Discussion

We showed that the branching of a hypothetical splay fault from the plate boundary during large subduction earthquakes can locally increase the maximum wave height by nearly a factor of 2. In our modeling, a slip of 10 m was supposed on the splay fault. It is evident that the larger the slip on the splay fault, the larger the runup height that is produced. The increase of the local runup by a factor of about 2 or more due to the splay faulting was previously documented by field surveys, e.g., the 2004 Indian Ocean tsunami (Plafker et al., 2007), the 1960 Chilean and 1964 Alaskan tsunami (Plafker, 1972). Therefore, for planning purposes, it seems reasonable and conservative to consider that the local runup may be at least twice the amount estimated from modeling studies. Based on this assumption, the two tsunami scenarios may produce a runup height of 12–18 m and 24–30 m, respectively. We add that a safety factor of 2 was previously applied for tsunami modeling results by Legg et al. (2004) in their tsunami hazard assessment for the southern California. Furthermore, the pronounced effect of splay faulting on the local runup height may highlight the need for future research to investigate which parts of the MSZ are likely to experience this phenomenon during large earthquakes.

For Fig. 3, we did not perform inundation calculations. Therefore, the runup heights presented in that figure should only be taken as a rough guide. Only where we performed a full analysis, including inundation modeling (e.g., Figs. 4 and 5), are our computed runup heights expected to match observations.

Our results were obtained without considering possible landslide generation during the two worst-case earthquakes. A landslide may have occurred during the 1945 Makran tsunami (Heidarzadeh et al., 2008a), and it is possible that the worst-case scenarios described here also could trigger submarine landslides. Several authors reported that submarine landslides can locally intensify the destructive effects of tsunami (e.g., Synolakis et al., 2001). Although landslides were not included in the tsunami scenarios, the safety factor of 2 proposed for the modeling results should account for the effects of possible landslides triggered by large earthquakes.

To further assess the veracity of the results, we compare them with those of a similar magnitude tsunami worldwide. In this context, the 2004 Indian Ocean tsunami serves as a good choice as its characteristics are close to those of our second scenario. As criteria for this comparison, we compare the ratio of the maximum runup to the average slip on the fault as well as the maximum inundation distances for the two cases (Table 4). The basis for this comparison is the study by Okal and Synolakis (2004) who have shown that, in the absence of major bathymetric irregularities, runup in the near-field is predicted to be no more than twice the seismic slip. However, we note that according to Kanoglu and Synolakis (1998), the maximum runup of long waves is very dependent on the local bathymetry and topography and especially on the last coastal topographic segment that the tsunami encounters. Also, this is the case for the maximum horizontal inundation of a tsunami that propagates over dry land. Therefore, it may not be appropriate to compare the maximum runup and inundation distance of a tsunami in a particular coastal site with those of another tsunami at another site. However, such comparisons are useful here, since both of our scenarios and the 2004 tsunami are worst-case events.

As stated by Okal and Synolakis (2008), the scenarios studied in this paper are extreme tsunami for the region, and do not necessarily represent the next great earthquake and tsunami in the northwestern Indian Ocean. We add that both tsunami scenarios, investigated in this study, are capable of producing significant effects in the far-field in the Indian Ocean basin. However, the far-field effects of worst-case earthquakes and resultant tsunamis were previously investigated by Okal and Synolakis (2008), and we do not investigate this further here.

The 2004 Indian Ocean tsunami showed that it is necessary to produce inundation maps depicting possible flooding zones from a variant of the December 26th, 2004 event everywhere across the Indian Ocean (Synolakis and Bernard, 2006). Inundation maps are necessary for the planning of mitigation strategies and should be based on the worst-case scenarios (Synolakis, 2003). Therefore, the results of this study are the first attempts towards the development of inundation maps for the northwestern Indian Ocean.

8. Conclusions

We have investigated the near-field effects of two worst-case scenario tsunami in the MSZ in order to give estimates of the possible effects of extreme tsunami in the northwestern Indian Ocean. The two scenarios included the rupture of about 500 and 900 km of the plate boundary featuring moment magnitudes of about M_w 8.6 and M_w 9, respectively. The main findings are:

1. The maximum seafloor uplift due to the first scenario earthquake was about 4.5 m. The resulting tsunami reached a height of about 6–9 m along the coast.
2. The first tsunami scenario produced large wave heights along the southern coast of Pakistan, and moderate heights on the remaining coasts.
3. The second scenario caused wave amplitudes of 12–15 m and horizontal penetration of about 1–5 km in various coasts. The

Table 4
Comparison of the maximum runup and inundation of the second scenario tsunami with those of the 2004 event.

Event	S = average fault slip (m)	R = maximum runup (m)	L = maximum inundation (km)	R/S
2004 tsunami	16[a]	32.5[b]	3–4[b]	2.0
Scenario 2	25	30	2–5	1.2

[a] Plafker et al. (2007); Geist et al. (2006).
[b] Synolakis and Kong (2006).

impact of this tsunami in the near-field was comparable to that of the 2004 Indian Ocean tsunami.

4. Modeling of a hypothetical splay fault showed that it can locally increase the maximum wave height by nearly a factor of 2. Hence, for planning purposes, we propose a safety factor of 2 for our results. Therefore, the two tsunami scenarios produce an average runup of 12–18 m and 24–30 m, respectively.
5. Our results verify previous statements by Heidarzadeh et al. (2008a) that secondary sources (e.g., splay faults and landslides) play an important role in intensifying runup heights in the near-field.
6. Although landslides were not included in the tsunami scenarios, the safety factor of 2 proposed for the modeling results should cover the impact of possible landslides triggered by large earthquakes.
7. We highlight the need to investigate which parts of the MSZ are likely to experience splay faulting as it was shown that this phenomenon has a pronounced effect on the local runup height.

Acknowledgements

Partial financial support was received from Intergovernmental Oceanographic Commission (IOC) of UNESCO in the form of a scholarship awarded to the first author. The long wave propagation model used in this study, TUNAMI-N2, is a registered copyright of Professors F. Imamura, A.C. Yalciner, and C. E. Synolakis. We thank Dr. William Fletcher from the University of Bordeaux 1 for his constructive review of the manuscript. This manuscript greatly benefited from constructive and detailed reviews by three anonymous reviewers. We are sincerely grateful to them for the comments that greatly improved this article.

References

Ambraseys, N.N., Melville, C.P., 1982. A History of Persian Earthquakes. Cambridge University Press, Cambridge, Britain, pp. 218.

Ando, M., 1975. Source mechanism and tectonic significance of historical earthquakes along the Nankai trough, Japan. Tectonophysics 27, 119–140.

Ben–Menahem, A., Rosenman, M., 1972. Amplitude patterns of tsunami waves from submarine earthquakes. Journal of Geophysical Research 77, 3097–3128.

Berninghausen, W.H., 1966. Tsunamis and seismic seiches reported from regions adjacent to the Indian Ocean. Bulletin of the Seismological Society of America 56 (1), 69–74.

Byrne, D.E., Sykes, L.R., Davis, D.M., 1992. Great thrust earthquakes and aseismic slip along the plate boundary of the Makran subduction zone. Journal of Geophysical Research 97 (B1), 449–478.

Cummins, P.R., Kaneda, Y., 2000. Possible splay fault slip during the 1946 Nankai earthquake. Geophysical Research Letters 27 (17), 2725–2728.

Geist, E., Titov, V., Synolakis, C., 2006. Tsunami: wave of change. Scientific American 294 (1), 56–63.

Goto, C., Ogawa, Y., Shuto, N., Imamura, F., 1997. Numerical method of tsunami simulation with the leap-frog scheme (IUGG/IOC Time Project), IOC Manual, UNESCO, No. 35.

Heck, N.H., 1947. List of seismic sea waves. Bulletin of the Seismological Society of America 37 (4), 269–286.

Heidarzadeh, M., Pirooz, M.D., Zaker, N.H., Yalciner, A.C., Mokhtari, M., Esmaeily, A., 2008a. Historical tsunami in the Makran subduction zone off the southern coasts of Iran and Pakistan and results of numerical modeling. Ocean Engineering 35 (8 & 9), 774–786.

Heidarzadeh, M., Pirooz, M.D., Zaker, N.H., Synolakis, C.E., 2008b. Evaluating tsunami hazard in the northwestern Indian Ocean. Pure and Applied Geophysics 165 (11–12), 2045–2058.

Heidarzadeh, M., Pirooz, M.D., Zaker, N.H., Yalciner, A.C., 2009. Preliminary estimation of the tsunami hazards associated with the Makran subduction zone at the northwestern Indian Ocean. Natural Hazards 48 (2), 229–243.

IOC, IHO, BODC, 2003. Centenary edition of the GEBCO digital atlas, published on CD-ROM on behalf of the Intergovernmental Oceanographic Commission and the International Hydrographic Organization as part of the general bathymetric chart of the oceans, British oceanographic data centre, Liverpool.

Kanoglu, U., Synolakis, C.E., 1998. Long wave runup on piecewise linear topographies. Journal of Fluid Mechanics 374, 1–28.

Legg, M.R., Borrero, J.C., Synolakis, C.E., 2004. Tsunami hazards associated with the Catalina fault in southern California. Earthquake Spectra 20 (3), 1–34.

Mansinha, L., Smylie, D.E., 1971. The displacement field of inclined faults. Bulletin of the Seismological Society of America 61 (5), 1433–1440.

McCaffrey, R., 2007. The next great earthquake. Science 315, 1675–1676.

Mokhtari, M., Abdollahie, I., Khaled Hessami, H., 2008. Structural elements of the Makran region, Oman sea and their potential relevance to tsunamigenesis. Natural Hazards 47, 185–199.

Okal, E.A., Synolakis, C.E., 2008. Far-field tsunami hazard from mega-thrust earthquakes in the Indian Ocean. Geophysical Journal International 172 (3), 995–1015.

Okal, E.A., 2007. Seismic records of the 2004 Sumatra and other tsunamis: a quantitative study. Pure and Applied Geophysics 164, 325–353.

Okal, E.A., Synolakis, C.E., 2004. Source discriminants for near-field tsunamis. Geophysical Journal International 158, 899–912.

Page, W.D., Alt, J.N., Cluff, L.S., Plafker, G., 1979. Evidence for the recurrence of large-magnitude earthquakes along the Makran coast of Iran and Pakistan. Tectonophysics 52, 533–547.

Plafker, G., 1972. Alaskan earthquake of 1964 and Chilean earthquake of 1960: implications for arc tectonics. Journal of Geophysical Research 77, 901–923.

Plafker, G., Ward, S.N., Nishenko, S.P., Cluff, L.S., Coonrad, J., Syahrial, D., 2007. Evidence for a secondary tectonic source for the cataclysmic tsunami of 12/26/2004 on NW Sumatra. Bulletin of the Seismological Society of America, Annual meeting, Kona, Hawaii, April 11–13. Abstract.

Quittmeyer, R.C., Jacob, K.H., 1979. Historical and modem seismicity of Pakistan, Afghanistan, northwestern India, and southeastern Iran. Bulletin of the Seismological Society of America 69 (3), 773–823.

Sibuet, J.C., et al., 2007. 26th December 2004 great Sumatra-Andaman earthquake: Co-seismic and post-seismic motions in northern Sumatra. Earth and Planetary Science Letters 263, 88–103.

Stein, S., Okal, E.A., 2007. Ultralong period seismic study of the December 2004 Indian Ocean earthquake and implications for regional tectonics and the subduction process. Bulletin of the Seismological Society of America 97 (1A), S279–S295.

Synolakis, C.E., 2003. Tsunami and seiche. In: Chen, W.F., Scawthorn, C. (Eds.), Earthquake Engineering Handbook. CRC Press, Boca Raton, FL, pp. 1–90 (Chapter 9).

Synolakis, C.E., Bernard, E.N., 2006. Tsunami science before and beyond Boxing Day 2004. Philosophical Transactions of the Royal Society A 364, 2231–2265.

Synolakis, C.E., Borrero, J.C., Kanoglu, U., Dolan, J., 2001. The slump origin of 1998 Papua New Guinea tsunami. Proceedings of the Royal Society of London 457, 1–27.

Synolakis, C.E., Kong, L., 2006. Runup measurements of the December 2004 Indian Ocean tsunami. Earthquake Spectra 22 (S3), S67–S91.

Tinti, S., Armigliato, A., Manucci, A., Pagnoni, G., Zaniboni, F., Yalciner, A.C., Altinok, Y., 2006. The generating mechanisms of the august 17th, 1999 Izmit Bay (Turkey) tsunami: regional (tectonic) and local (mass instabilities) causes. Marine Geology 225, 311–330.

Titov, V.V., Synolakis, C.E., 1997. Extreme inundation flow during the Hokkaido-Nansei-Oki tsunami. Geophysical Research Letters 24, 1315–1318.

Wells, D.L., Coppersmith, K.J., 1994. New empirical relationships among magnitude, rupture length, rupture width, rupture area, and surface displacement. Bulletin of the Seismological Society of America 84 (4), 974–1002.

Yalciner, A.C., Pelinovsky, E., Talipova, T., Kurkin, A., Kozelkov, A., Zaitsev, A., 2004. Tsunamis in the Black Sea: comparison of the historical, instrumental, and numerical data. Journal of Geophysical Research 109 (12), 2003–2113.

Yeh, H., Liu, P., Synolakis, C.E., 1996. Long Wave Runup Models. World Scientific Publication Company, London, pp. 403.